Brittle fracture in materials with random defects

G. N. Hassold and D. J. Srolovitz
Department of Materials Science and Engineering, University of Michigan, Ann Arbor, Michigan 48109
(Received 27 December 1988)

We study the failure properties of a defected square lattice of Born springs under uniaxial tensile strain. The springs fail completely and irreversibly once a critical strain energy is exceeded. The Born potential provides an effective bending force that yields realistic crack microstructures, which are analyzed in detail. As the defect density increases, the crack becomes increasingly ramified, even though fewer spring failures are required for complete breakdown. The failure stress and Young's modulus approach zero as the system approaches the percolation threshold. Cumulative failure-stress distributions appear consistent with both Weibull and Duxbury-Leath forms. The size and composition of the crack (in terms of initial defects and broken springs) are analyzed as functions of defect density, lattice size, and bending constant.

I. INTRODUCTION

The fracture properties of materials are known to depend sensitively on the microstructure.[1] In metals, the important microstructural components include grain boundaries and second-phase particles. The second-phase particles may provide crack-nucleation sites and the grain boundaries, if sufficiently weak, provide easy crack-propagation paths. In brittle materials, such as many ceramics and minerals, similar considerations are important. However, in such cases the fracture properties are usually dominated by the size and spatial distributions of flaws or microcracks, which are often artifacts of processing conditions. Recently, a great deal of attention has been focused on the role of random distributions of flaws on failure properties.[2-6] These failure studies have focused on fracture,[2-4] dielectric breakdown,[5] failures of random-fuse networks,[6] etc. The present study focuses on the fracture of an elastic network with randomly distributed defects. Unlike previous studies which concentrate on critical properties and the distribution of the failure stress,[2-4] this work also considers the properties of the crack cluster as a method of independently investigating the role of the distribution of defects in crack nucleation and crack propagation.

One commonly used approach in simulating failure in elastic systems is to represent the elastic medium as a network of Hookean springs.[7] The potential energy of the spring connecting two sites, α and β, is

$$\Phi_{\alpha\beta}=\tfrac{1}{2}k_{\alpha\beta}(|\mathbf{x}_\beta-\mathbf{x}_\alpha|-a_{\alpha\beta})^2 , \quad (1)$$

where $k_{\alpha\beta}$ is the spring constant for the spring connecting sites α and β, $a_{\alpha\beta}$ is its equilibrium separation, and x_α (x_β) the position of site $\alpha(\beta)$. Fracture is simulated[4] by assuming that if the strain $[\varepsilon_{\alpha\beta}=(x_\beta-x_\alpha)/a_{\alpha\beta}]$ in any spring exceeds a predefined breaking strain ε_b, the spring would break irreversibly and $k_{\alpha\beta}$ would be set to zero. This approach has been used to calculate[2-4] scaling laws, critical properties, failure stresses for dilational and uniaxial strains, failure-stress distributions, etc.

While the Hookean-spring model is very simple, it does have a number of problems. Unlike most real materials, this model has a zero Poisson ratio for a square lattice. This physically unreasonable feature is attributable to the fact the springs are free to rotate about the nodes at which the springs meet. Although the two-dimensional triangular lattice has a finite Poisson ratio, the free rotation of the springs about their nodes still presents problems. Fracture in such models often occurs by the failure of a continuous path of springs parallel to the applied stress, followed by the stress-free rotation of surviving springs into a load-bearing orientation and subsequent fracture along the same path.[3,4] Such preshearing of the lattice may be appropriate to problems where plastic deformation is important, but is an undesirable property for models of brittle materials.

The disadvantages of the Hookean-spring model have been overcome in a number of different ways. The first is to add a term to the Hamiltonian which penalizes bond bending (i.e., a three-body term).[8] A second is to replace the spring lattice with two-dimensional elements (based on Hookean springs), which results in two independent Lamé constants.[9] A third approach is to employ Born springs (described below), which penalize rotation of the springs away from lattice directions.[10,11] This approach is much simpler than the two-dimensional–element approach, while still yielding two independent Lamé constants. Unfortunately, this model is not rotationally invariant.[12] This, however, does not present any problems in cases where the spring-breaking strain ε_b is very small.

The present study employs a Born-spring model to study the effects of a random distribution of defects on the fracture of an elastic model loaded in pure tension. The next section of this paper defines the Born model and the simulation method employed in the fracture study. Section III shows the microstructure development during failure and the resulting crack morphologies as a function of the initial defect density. The stress-strain curves appropriate to these morphologies, the failure-stress distribution functions, and an investigation of model parameters comprise the subject of the next two sections. Final-

ly, the effect of model parameters and initial defect density on the fracture path are shown.

II. THE BORN MODEL

Rather than add a (three-body) bending force to the spring model used above, we have chosen to work with a similar potential which incorporates the desired features. The potential, due originally to Born,[10] is given by

$$\Phi_{\alpha\beta}=\tfrac{1}{2}(k_{\alpha\beta}-c_{\alpha\beta})[(\mathbf{u}_\beta-\mathbf{u}_\alpha)\cdot\hat{\mathbf{r}}_{\alpha\beta}]^2+\tfrac{1}{2}c_{\alpha\beta}|\mathbf{u}_\beta-\mathbf{u}_\alpha|^2 , \quad (2)$$

where k and c are constant potential parameters, u represents a displacement from an equilibrium position, and $\hat{\mathbf{r}}$ is the unit vector corresponding to the direction between sites α and β in the perfect lattice. The parameters k and c are generally site dependent; initially we will remove this dependence, except for setting the parameters of broken springs to zero. This potential may be more clearly written for a square lattice, upon which our calculations will be performed. If sites α and β are neighboring in the x direction, the potential term is

$$\Phi_{\alpha\beta}=\tfrac{1}{2}k_{\alpha\beta}(|x_\beta-x_\alpha|-a_{\alpha\beta})^2+\tfrac{1}{2}c_{\alpha\beta}(y_\beta-y_\alpha)^2 , \quad (3)$$

where x_α and y_α are the x and y positions of site α, and $a_{\alpha\beta}$ is the equilibrium separation of sites α and β. If α and β are neighboring in the y direction, the above formula is modified by the substitution of x for y, and vice versa. The first term in the potential function accounts for spring stretching with a spring constant k, which penalizes deviations from the equilibrium spacing along the preferred spring direction. The second term accounts for the deviation of the spring from its preferred direction by inclusion of an additional spring with spring constant c. For small deviations this can be thought of as a bond-bending term. It prevents the stressless elongation of the lattice due to bond rotation (as observed in the case of classical springs). The formulation of this bending term lacks rotational invariance.[12] The lack of rotational invariance is unimportant in the present study, since springs break at very small strain. Unlike in the spring-model study,[4] where a strain-failure criterion was used (a spring breaks when $\varepsilon_{\alpha\beta}>\varepsilon_b$), we use an energy-failure criterion for the Born springs (a spring breaks when its strain energy $\Phi_{\alpha\beta}>\Phi_b$).

In the present work this potential is used for the Born springs in a two-dimensional square lattice, whose length will be denoted by L. The spring constant k has been set to 1, c/k is varied, and the breaking energy Φ_b is set to 5.0×10^{-5}. Periodic boundary conditions are applied along the two surfaces of the square model whose normals are parallel to the applied load, which is taken to be the x direction. In order to study the effects of a random distribution of defects, a fraction $1-p$ of the initial springs are cut (locations chosen at random). An initial, infinitesimal strain is applied, and the lattice is equilibrated by balancing forces on the (static) nodes. The total stress and strain are then calculated, as well as the energy of each spring. Since the system behaves linearly between spring failures, the strain (ε_f^*) and stress (σ_f^*) at which the first spring will fail are given by

$$\varepsilon_f^*=\varepsilon(\Phi_b/\Phi_m)^{1/2} , \quad (4)$$

$$\sigma_f^*=\sigma(\Phi_b/\Phi_m)^{1/2} , \quad (5)$$

where Φ_m is the maximum energy in any individual spring, and σ and ε are the total stress and strain, respectively. The strain is then set infinitesimally above ε_f^*, and the most energetic spring (previously determined) is broken. The lattice is then successively reequilibrated and the spring with the maximum Φ is cut (provided $\Phi>\Phi_b$), until no further springs fail at that strain level. The new stress and maximum spring energy are again measured, and used in the above formula to predict the next failure strain and stress. This process of relaxation (successive equilibration and spring breaking) and strain incrementation is continued until the entire sample fails.

III. MICROSTRUCTURE

Figure 1 displays the configuration of a 25×25 lattice for $c/k=0.1$ and $p=0.995$ following its failure at a stress of $\sigma_f=0.743$ and a strain of $\varepsilon_f=0.765$ (note the quoted failure strains and stresses throughout have been normalized to those in the perfect lattice). Springs that break during the simulation are indicated by dashed lines and those that were cut prior to the application of the strain are missing. The crack nucleates at a single precut spring and then propagates through the entire sample in the direction normal to the applied load with no further increase in stress or strain (i.e., the system fails catastrophically). The failure path is nearly straight, except for a single kink that the crack makes in order to take advantage of a precut spring which was near the advancing crack tip.

A sequence of failure configurations for $p=0.9$ is shown in Fig. 2. The first spring breaks at $\sigma=0.344$ and

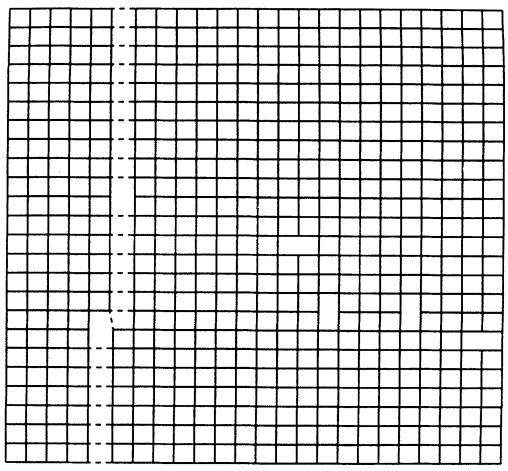

FIG. 1. Failure configuration of a 25×25 lattice of Born springs, for $p=0.995$ and $c/k=0.1$. Springs which fail during elongation are shown as dashed lines.

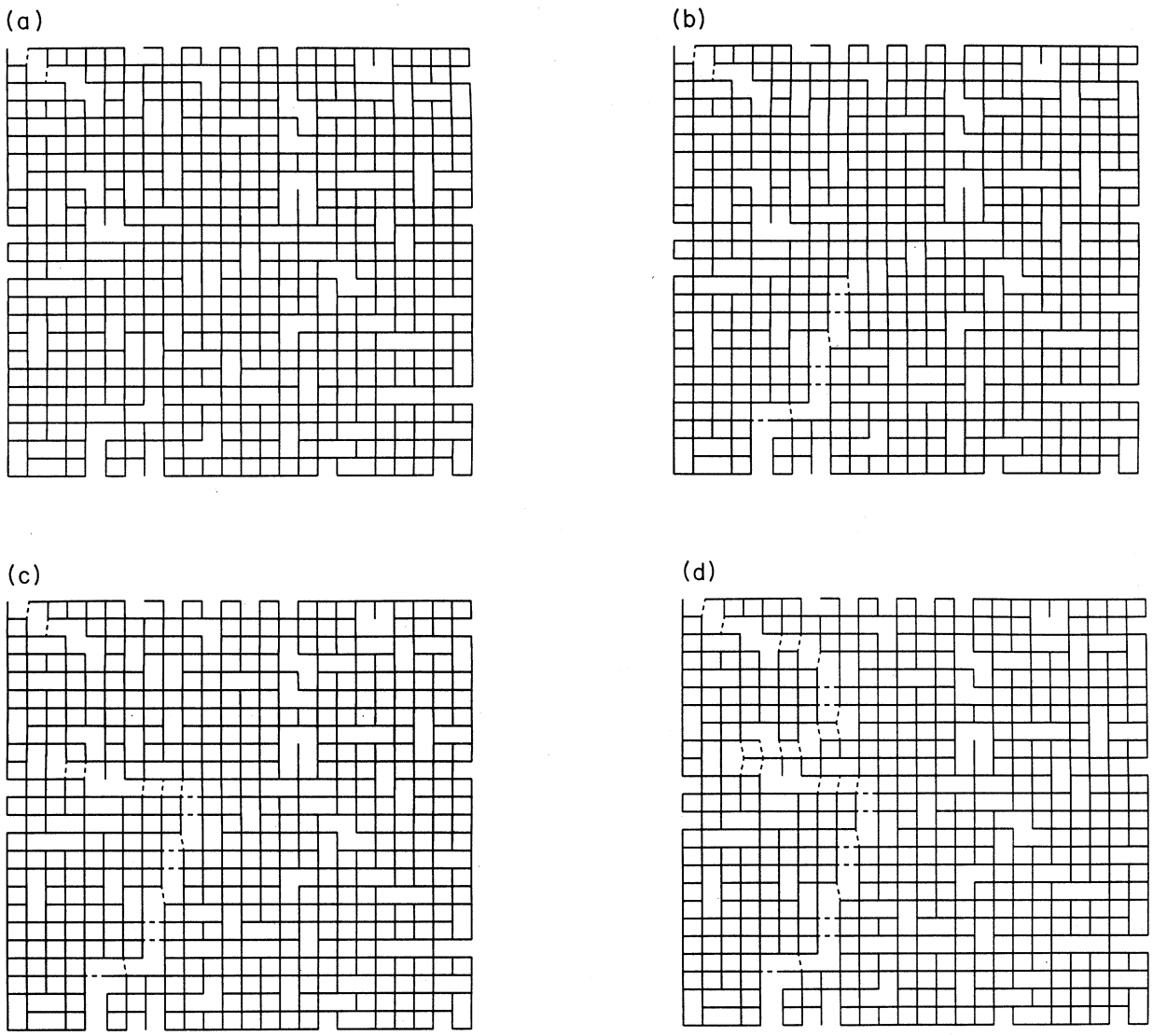

FIG. 2. Failure of a 25×25 lattice for $p=0.9$, $c/k=0.1$: (a) initial failure, $\varepsilon=0.594$; (b) $\varepsilon=0.597$; (c) $\varepsilon=0.621$; (d) final failure, $\varepsilon=0.665$.

$\varepsilon=0.594$ [Fig. 2(a)]. Unlike the $p=0.995$ case previously discussed, the sample does not fail instantaneously when the first spring breaks. Further increases in the applied strain lead to additional noncatastrophic failures [Figs. 2(b) and 2(c)]. These additional breaks occur at stress levels lower than that for the initial spring failure. The sample finally fails at $\varepsilon=0.665$ [Fig. 2(d)]. Also, in contrast to the $p=0.995$ case, the final failure path for $p=0.9$ is far from straight. This apparent wandering of the advancing crack tip may be attributed to the relatively large number of nearby precut springs.

The effects of increased initial defect density is shown in Figs. 3(a)–3(c), where the failure configurations correspond to $p=0.8$, 0.7, and 0.6, respectively. Clearly, as the initial defect density is increased the failure path becomes increasingly tortuous. The number of springs in the failure path also appears to increase with decreasing p. At the same time, the number of springs which are broken during the failure event decreases with decreasing p. In the limit that $p \rightarrow p_c$ (the percolation threshold), the failure path would contain a number of springs which would scale as L^d, where d is the fractal dimension of the random percolation cluster ($d \approx 1.9$), and the number of springs broken during the failure approaches zero. The failure stress decreases with increasing initial defect density toward a value of zero at p_c.

IV. STRESS-STRAIN BEHAVIOR

The stress-strain curves corresponding to the microstructures shown above are presented in Fig. 4. The most

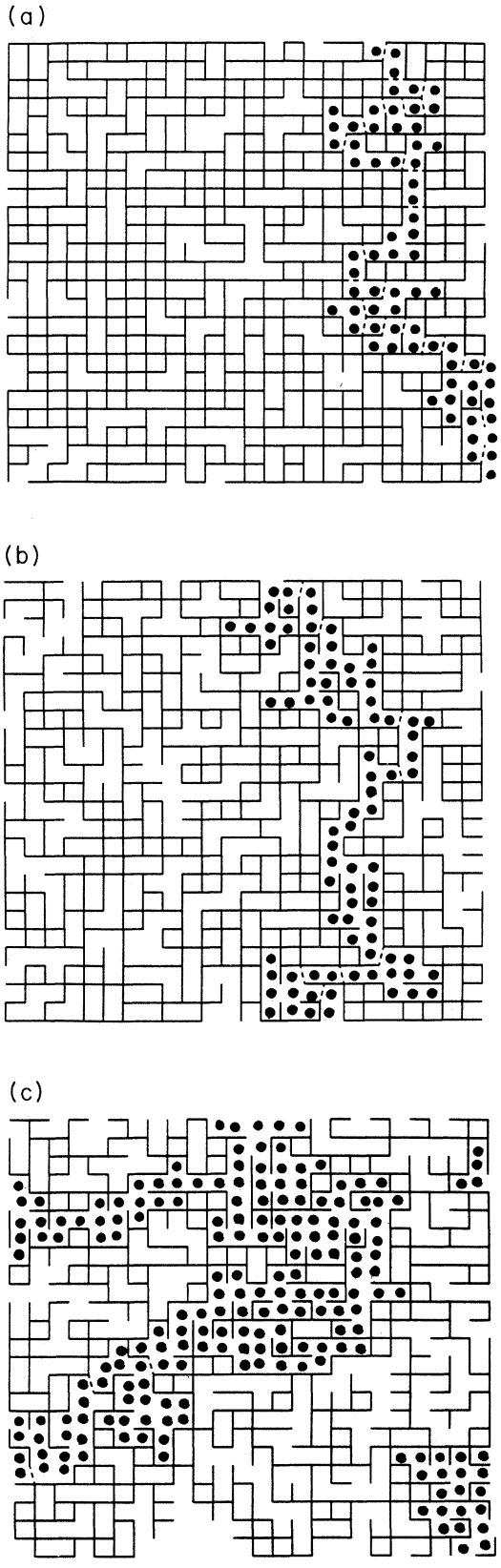

FIG. 3. Final-failure configurations for a 25×25 lattice with $c/k=0.1$, for (a) $p=0.8$; (b) $p=0.7$; (c) $p=0.6$.

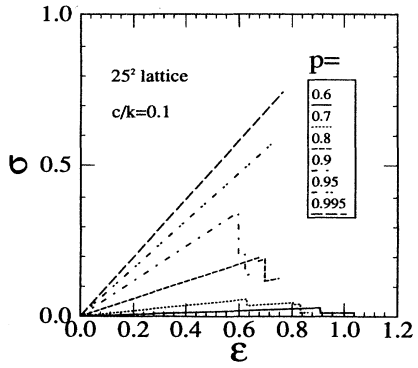

FIG. 4. Stress-strain curves corresponding to Figs. 1–3 (25×25 lattice, $c/k=0.1$).

striking feature of these curves is that the slopes decrease with decreasing p. These slopes correspond to the elastic (Young's) modulus, E, of the samples. Figure 5(a) shows this trend quantitatively. The modulus data are based upon 400 simulations, and the error bars represent the inherent width of the distribution (i.e., the standard deviation of the sample). The modulus clearly tends to zero as $p\rightarrow p_c$ (the rigidity percolation threshold for the Born model with $c/k>0$ is identical to the normal percolation threshold). It should also be noted that the dependence of E on $p-p_c$ is decidedly nonlinear, as opposed to the linear behavior seen previously in the spring model.[4]

There are several valid definitions of the failure stress, depending on the nature of the tensile test. In a stress-controlled test the stress is incremented, and the strain is the dependent variable. In this case the sample fails at the highest stress value in the stress-strain curve, σ_f^{σ}. This usually occurs at the point where the first spring breaks. In a strain-controlled test, on the other hand, the strain is incremented and the stress is the dependent variable. As the stress is finite for all strains, the failure stress in this case corresponds to the point where the stress first drops to zero, σ_f^{ε}. Figure 4 shows that the main-controlled failure stress is always less than or equal to the stress-controlled failure stress. Similarly, the strain at which failure occurs in a stress-controlled test is always less than or equal to that for a strain-controlled test.

The dependence of the failure stress on p is shown in Fig. 5(b). Both σ_f^{σ} and σ_f^{ε} decrease monotonically with increasing defect density (decreasing p) and tend toward zero as $p\rightarrow p_c$. The error bars show that the width of the distribution of the strain-controlled failure stresses greatly exceeds that for the stress-controlled case. Also plotted in this figure is σ_1, which is the stress at which the first spring breaks. Comparison of the curves for σ_f^{σ} and σ_1 demonstrates that in stress-controlled tests the failure of the system is usually coincident with the failure of the first spring. The agreement is best as $p\rightarrow1$ or $p\rightarrow p_c$ (where they are constrained to be equal), with only slight deviations at intermediate values. Therefore σ_1 provides a good estimate for σ_f^{σ}, at considerable computational savings.

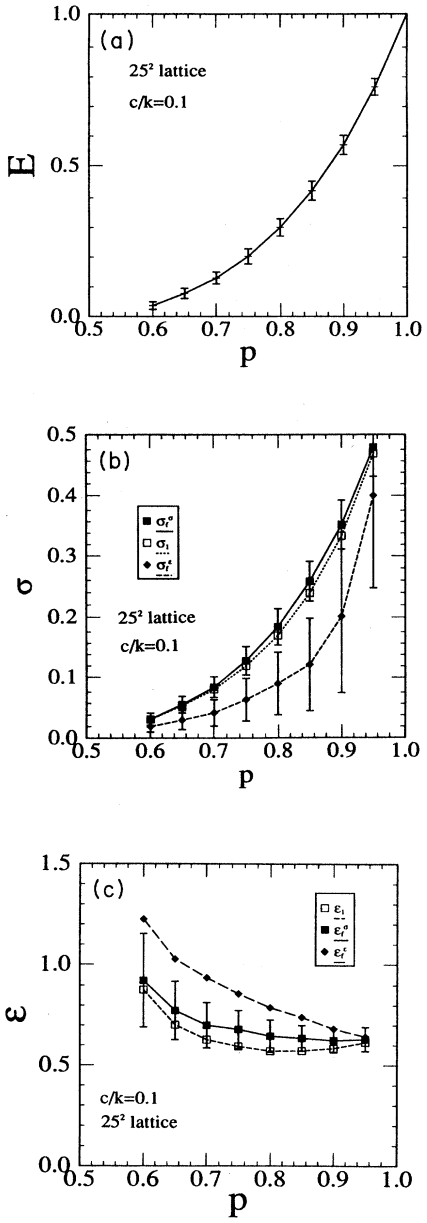

FIG. 5. Effect of defect density $(1-p)$ on (a) Young's modulus, (b) failure stress, and (c) failure strain. All values are normalized to those of a perfect lattice.

Figure 5(c) displays the effect of p on the failure strain. The failure strain clearly increases with increasing defect density. This suggests that the ductility (strain to failure) of this microscopically elastic model increases with increasing defect density, albeit at the expense of increased damage. As $p \rightarrow 1$, ϵ_f must go to unity. This must be attributed to the fact that a single defect in a large sample has a much more pronounced effect on the failure stress than on the Young's modulus.

The dependence of the failure stress and of Young's modulus on c/k are shown in Figs. 6(a) and 6(b). As c/k

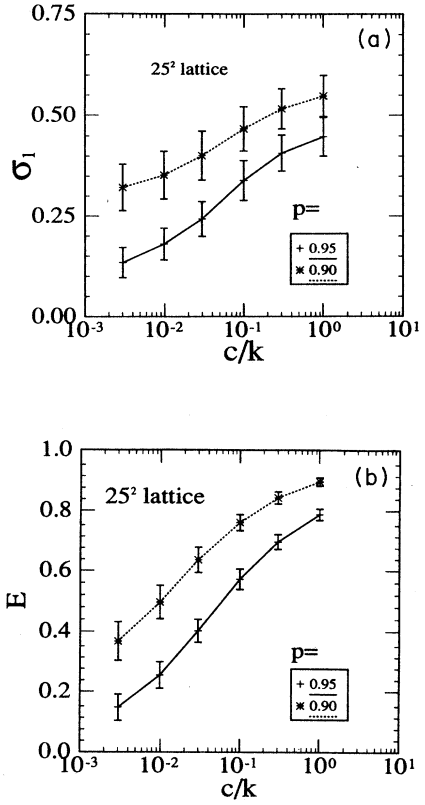

FIG. 6. Effect of c/k on (a) failure stress and (b) Young's modulus.

decreases the interaction between the individual rows of springs (parallel to the applied stress) lessens. In the limit that $c/k \rightarrow 0$ the rows of springs can slide by each other without hindrance. As a result, one broken spring anywhere in each row would be sufficient to mechanically disconnect the sample and, hence, σ_f and E both go to zero as $c/k \rightarrow 0$ in an infinite lattice. In the opposite limit $(c/k \rightarrow \infty)$ the model is insensitive to elongation and, hence, the failure stress tends to infinity. Clearly, a value of c/k appropriate to the failure of elastic bodies must lie between these two extremes. Since the properties of the lattice change slowly with c/k, and $c/k = 0.1$ clearly lies in the transition region between the two unphysical extremes, we arbitrarily set c/k to 0.1 for the present simulations. Figures 7(a) and 7(b) show the dependence of the failure stress and Young's modulus on the linear system size L. The Young's modulus is clearly independent of L, although the width of its distribution is not. The failure stress decreases with increasing L. This is to be expected as the likelihood of finding a large defect in a randomly defected sample increases with sample size. We typically employ $L = 25$ in the present simulations.

V. FAILURE-STRESS DISTRIBUTION

The cumulative distribution function for failure stresses $F_L(\sigma_1)$ is plotted in Fig. 8. We have used the

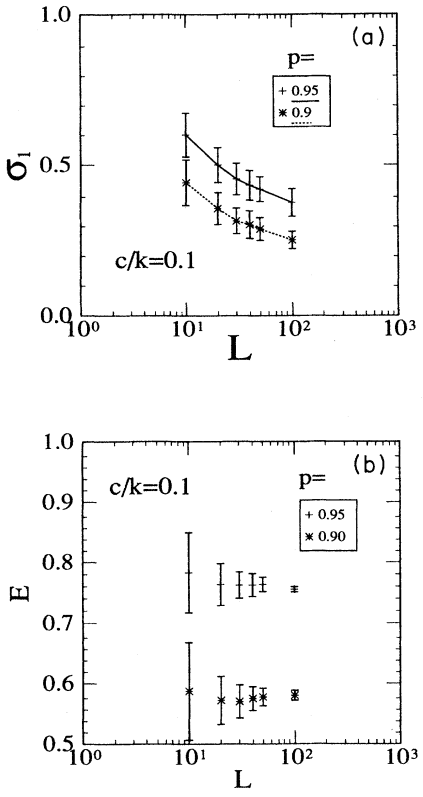

FIG. 7. Dependence of (a) failure stress and (b) Young's modulus on the linear system size, L.

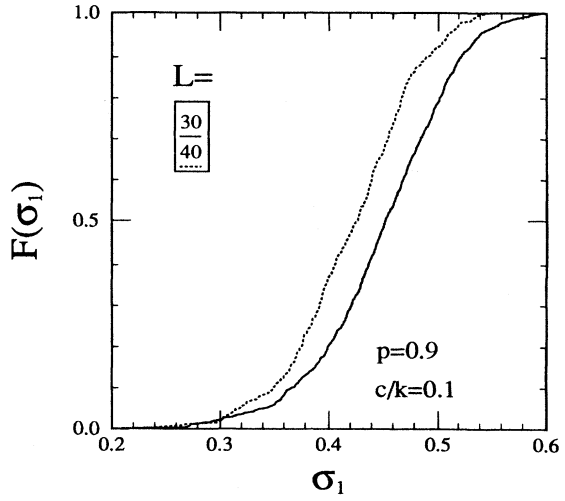

FIG. 8. Cumulative failure-stress distribution $F_L(\sigma_1)$ for $p=0.9$, $c/k=0.1$.

failure stress of the first spring (σ_1) as an estimate of the (stress-controlled) failure stress (σ_f^{σ}); as noted previously, this is an excellent approximation and allows us to gather greater statistics in an equivalent amount of time. The data represent 1000 trials on a 30×30 lattice and 500 trials on a 40×40 lattice. In order to test for conformity to a Weibull[13] distribution $[F_L(\sigma)=1-\exp(-cL^2\sigma^m)]$, in Fig. 9(a) we plot $-\ln\{-\ln[1-F_L(\sigma_1)/L^2]\}$ against $-\ln(\sigma_1)$. The straight line in this figure is the best fit to the $L=40$ data. The agreement between the simulation results and the Weibull distribution is good. The slope of this line corresponds to a Weibull modulus $m=10$. Such large Weibull moduli are not atypical for brittle materials.

Duxbury and Leath[14] have predicted an alternate form of the distribution function, valid away from the percolation threshold: $F_L(\sigma)=1-\exp[-cL^2\exp(-k/\sigma^{\mu})]$, with $1\le\mu\le2$. A plot of $-\ln\{-\ln[1-F_L(\sigma_1)/L^2]\}$ versus $1/\sigma^{\mu}$ should yield a straight line. This is done for $\mu=1$ in Fig. 9(b) and $\mu=2$ in Fig. 9(c). Again, the straight lines represent a best fit to the $L=40$ data. The agreement between the simulation data and the Duxbury-Leath distribution function is good for $\mu=1$ and rather poor for $\mu=2$. The Duxbury-Leath ($\mu=1$) distribution shows marginally better agreement with the data than the Weibull form for the $L=40$ data, but worse agreement for the $L=30$ data. Based upon our limited statistics in the tails of the distributions, it is not possible to make a useful distinction between the two distributions. These results are in mild disagreement with earlier simulations[4] on the linear-spring model (no bond-bending forces), where the Duxbury-Leath distribution appeared superior to the Weibull form.

VI. MICROSTRUCTURAL CHARACTERIZATION

In order to discuss the effect of model parameters on crack morphology, we must define a number of variables, which characterize the failed lattice. A spring is referred to as "cut" if it is one of the $(1-p)L^2$ springs removed prior to the simulation, and as "broken" if it fails as the strain is incremented. We can define a failure path or failure cluster by considering the perpendicular bisectors (dual springs) of all broken springs (the nodes where these bisectors meet are on the dual lattice). The fracture path is the connected cluster of dual springs that span the width of the sample. The total numbers of broken and cut springs are denoted N_b and N_c, respectively. The latter is simply equal to $L^2(1-p)$. The numbers of broken and cut springs *in* the crack are denoted by n_b and n_c, respectively. N_b and n_b need not be equal; a small number (n_b') of broken springs are not to be connected to the failure path.

The dependence of crack morphology on c/k is measured in several ways in Fig. 10. The crack size ($n=n_c+n_b$) is seen to decrease with increasing bending force, approaching the value of L for large c/k. The number of broken springs in the failure (crack) cluster also decreases, due to the decreasing crack size. The ratio of cut to broken springs (near unity for this choice of p) appears insensitive to c/k. Note that the value of $c/k=0.1$, employed above, lies between the stretching- and bending-dominated extremes.

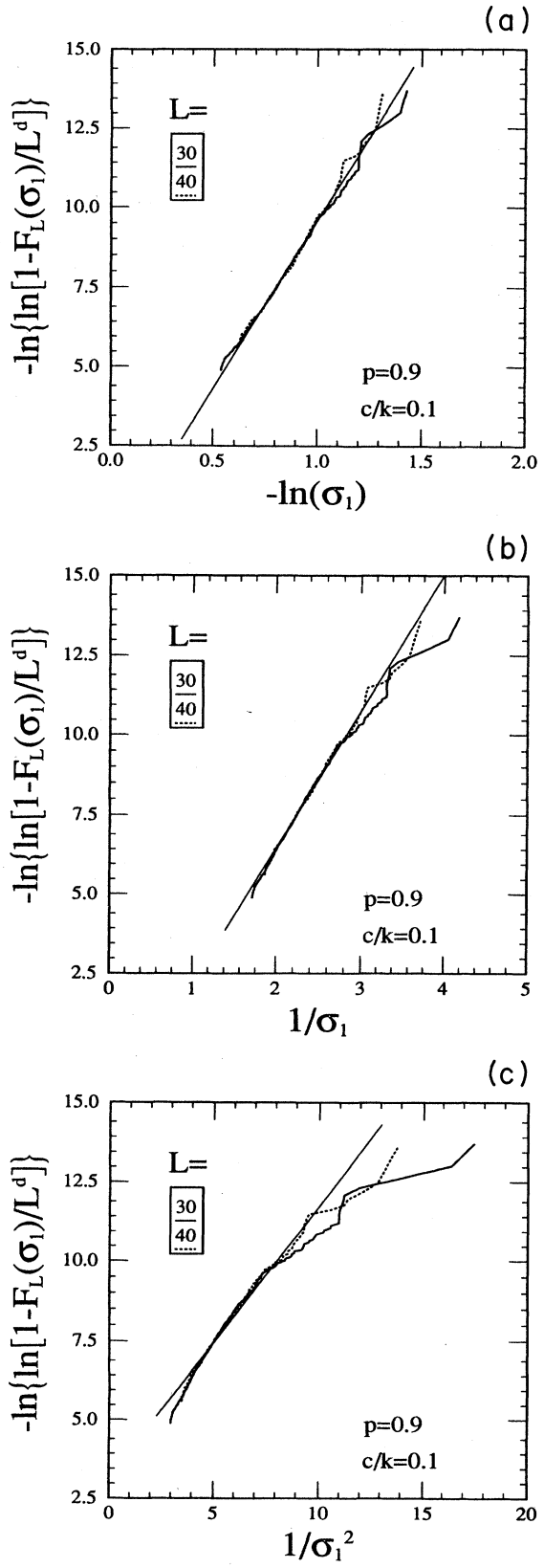

FIG. 9. Test plots for validity of the (a) Weibull distribution, (b) Duxbury-Leath $\mu=1$ distribution, and (c) Duxbury-Leath $\mu=2$ distribution.

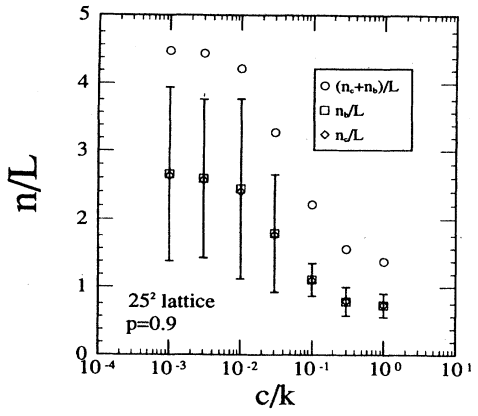

FIG. 10. Effect of c/k on crack morphology. n_b and n_c are the number of broken and cut bonds in the crack, respectively.

The scaling behavior of the crack-cluster statistics with L is shown in Fig. 11 for $p=0.9$. The number of broken springs within the crack scales with L with an exponent of 1.106 ± 0.007. The L dependence of the number of cut springs within the crack (n_c), and thus the crack size (n_b+n_c), are similar, with exponents of 1.103 ± 0.014 and 1.123 ± 0.011, respectively.

Figures 12(a) and 12(b) display the effect of defect density on the crack. For $p\rightarrow1$ the (straight) crack is made up almost entirely of broken springs, whose number equals the lattice width. The crack size (n_b+n_c) is seen [Fig. 12(a)] to increase dramatically with increasing defect density ($1-p$). This results from the increasingly tortuous nature of the crack, as shown in Figs. 1–3. At the percolation threshold only a few springs are holding the lattice together, and the resultant crack is composed almost entirely of cut springs. The number of broken

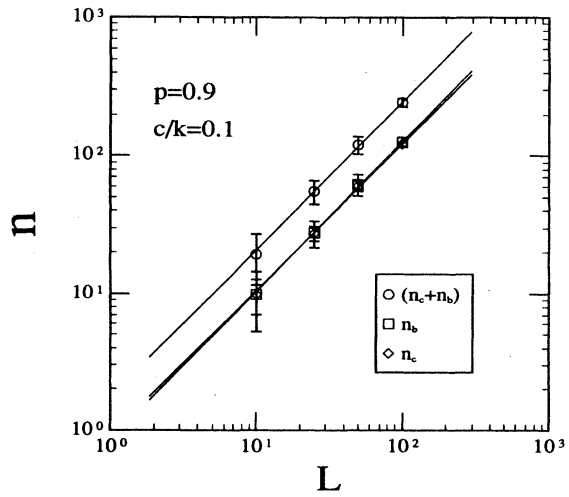

FIG. 11. Effect of linear system size L on crack morphology.

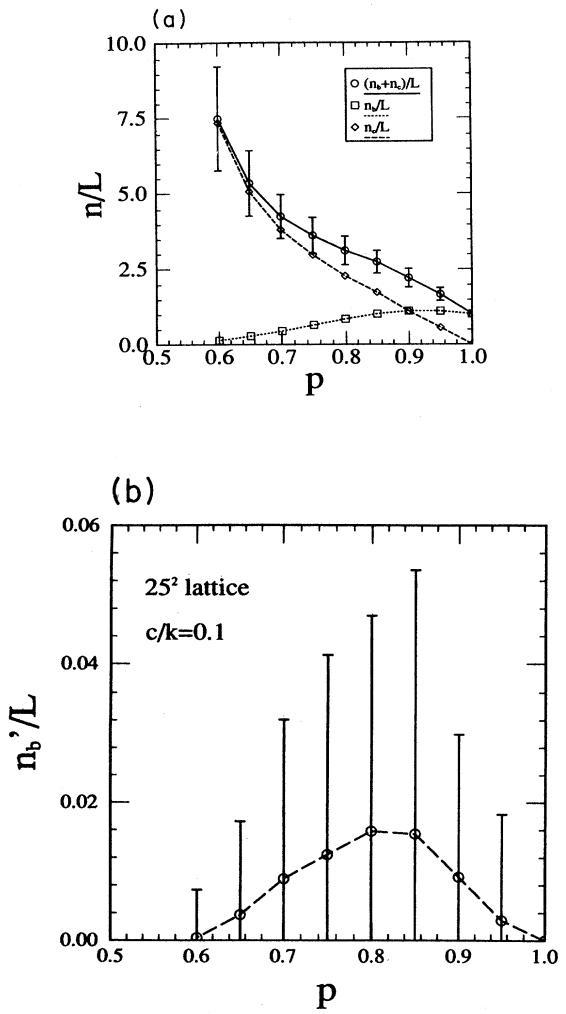

FIG. 12. Effect of defect density $(1-p)$ on crack morphology: (a) number of broken (n_b) and cut (n_c) bonds within the crack; (b) number of broken bonds outside the crack (n_b').

springs (n_b) shows the competition between these two effects. From an intermediate p maximum, n_b decreases as $p \to 1$ due to the straightening of the crack, and also decreases to zero as $p \to p_c$ due to the increased availability of cut springs. The number of broken springs [Fig. 12(b)] outside the crack (n_b') shows a more pronounced maximum. As p approaches unity, the first spring to break results in the catastrophic failure of the entire sample—hence, no springs break outside the failure cluster. In the limit that $p \to p_c$ the total number of broken springs tends to zero. Therefore, the maximum at intermediate p corresponds to those cases in which the stress-strain curve shows several load drops corresponding to several isolated failures in different regions of the material. When the critical crack starts to grow, it is unable to incorporate all of the isolated previously broken regions of the sample.

VII. DISCUSSION AND SUMMARY

In the tensile-fracture studies presented previously, the crack clusters which eventually lead to the failure of the sample are predominantly oriented in the direction normal to the applied stress. Such a result is clearly expected for tensile loading for nearly perfect samples. Two major effects are noticed as the initial defect density is increased. First, the failure stress drops. This can be attributed primarily to the larger defects (clusters of initially cut springs) present with increasing system size, as indicated by the scaling of the failure stress with L. The second effect is on the crack morphology. As p decreases (the initial defect density increases), the cracks look increasingly ramified. In the $p=1$ (no defect) limit the crack is straight (i.e., a fractal dimension D equal to the Euclidean dimension $d-1$). In the limit that $p \to p_c$ the fractal dimension of the crack must be equal to the fractal dimension of the percolation cluster ($D \approx 1.9$). For p between these two limits, our limited data suggest that an intermediate fractal dimension applies ($D \approx 1.1$ for $p=0.9$). We believe that this fractal dimension should be viewed as a crossover effect. Similar results with $D > d$ have been obtained in models for which dilational and shear strains were applied.[3]

The number of springs that must be broken for the crack to propagate across the entire sample generally decreases with increasing initial defect density. Likewise, the number of precut springs that are part of the crack increases with increasing defect density. Both of these effects are attributable to the crack being able to find more advantageously located defects in the vicinity of its tip with increasing defect density. A corollary to this is that a crack grows by larger increments with increasing defect density. This may be seen in the stress-strain curves (Fig. 4), where a great deal of strain must be applied between subsequent load drops (i.e., a larger strain is required to raise the stress at the tip of a long crack to the failure point than for a short crack). Examination of the failed samples (Figs. 1–3) shows that as the defect density increases a greater fraction of the broken springs are oriented such that they fail in shear [cf. Fig. 1 with Figs. 3(b) and 3(c)]. This suggests that the failure path is one that minimizes the number of springs which fail in tension. This is somewhat surprising, since for $c/k < 1$ a spring fails at smaller strain values in tension than in shear.

The failure-strain data show a marked difference between stress- and strain-controlled fracture. Considerably more strain may be accommodated under strain-control conditions than under stress-control conditions, especially at large defect densities. Although the ductility (strain to failure) is largest at low p, the energy absorbed on fracture (i.e., the toughness) and the fracture stress is smaller. The dependence of the stress at fracture is strongly dependent on testing mode. Nonetheless, the stress required for fracture is independent of the mode of testing. Comparison of the actual failure stress and that obtained by assuming that failure occurs as soon as a single spring breaks (σ_1) shows that σ_1 provides a good estimate of the actual failure stress. However, the deviation

between the measures of the strain to failure (stress controlled) shows that the sample often does not fail immediately following the first break, but fails at a stress near the first-break level. The widths of the distributions of stresses at fracture [see the error bars in Fig. 5(b)] are much sharper in stress control than in strain control. This suggests that the maximum stress on the stress-strain curve is a more fundamental quantity than is the stress at failure (in strain control).

The failure statistics from the present simulation employing Born springs is in excellent agreement with that obtained using Hookean springs.[4] This result suggests the near equivalence of the two models when dealing with elastic effects, including the failure stress since σ_1 ($\approx\sigma_f^{\sigma}$) is determined by the elastic properties. Nonetheless, the two models are *not* interchangeable with regard to crack morphology. Comparison of the cracks resulting from tensile tests in the two models (cf. Figs. 1 and 2 with Fig. 1 of Ref. 4) shows that the Hookean model cracks at a substantially different angle (with respect to the applied stress) than the Born model. Although these two simulations were performed on different lattices, we believe the differences transcend the lattice effect. We suggest that the energy must include terms which resist bond bending in order to obtain reasonable crack morphologies.

ACKNOWLEDGMENTS

We gratefully acknowledge Bill Visscher of Los Alamos National Laboratory for suggesting the Born model as a remedy for certain deficiencies of the Hookean-spring model, and the U.S. Department of Energy for its support through Contract No. DE-FG02-88ER45367.

[1] *Fracture,* edited by H. Leibowitz (Academic, New York, 1984), Vols. I–VII.

[2] R. F. Smalley, Jr. D. L. Turcott, and S. A. Soloa, J. Geophys. Res. **90**, 1894 (1985); B. K. Chakrabarti, D. Chowdury, and D. Stauffer, Z. Phys. B **62**, 344 (1986); P. Ray and B. K. Chakrabarti, Solid State Commun. **53**, 477 (1985); J. Phys. C **18**, L185 (1985); M. Sahimi and J. D. Goddard, Phys. Rev. B **33**, 7848 (1986); L. de Arcangelis, A. Hansen, H. J. Herrmann, and S. Roux (unpublished).

[3] P. Meakin, Thin Solid Films **151**, 165 (1987); E. Louis and F. Guinea, Europhys. Lett. **55**, 2688 (1987); P. Meakin, G. Li, L. M. Sander, E. Louis, and F. Guinea (unpublished).

[4] P. D. Beale and D. J. Srolovitz, Phys. Rev. B **37**, 5500 (1988).

[5] H. Takayasu, Phys. Rev. Lett. **54**, 1099 (1985); P. D. Beale and P. M. Duxbury, Phys. Rev. B **37**, 2785 (1988).

[6] P. M. Duxbury, P. L. Leath, and P. D. Beale, Phys. Rev. B **36**, 367 (1987); L. de Arcangelis, S. Redner, and H. J. Herrmann, J. Phys. (Paris) Lett. **46**, L585 (1985); B. Kahng, G. G. Batrouni, S. Redner, L. de Arcangelis, and H. J. Herrmann, Phys. Rev. B **37**, 7625 (1988).

[7] R. Hooke, *De Potentia Restitutiva* (London, 1678).

[8] L. M. Schwartz, S. Feng, M. F. Thorpe, and P. N. Sen, Phys. Rev. B **32**, 4607 (1985).

[9] R. Garcia-Molina, F. Guinea, and E. Louis, Phys. Lett **60**, 124 (1988).

[10] M. Born and K. Huang, *Dynamical Theory of Crystal Lattices* (Oxford University Press, New York, 1954).

[11] P. N. Sen and M. F. Thorpe, Phys. Rev. B **15**, 4030 (1977); S. Feng and P. N. Sen, Phys. Rev. Lett. **52**, 216 (1984).

[12] P. N. Keating, Phys. Rev. **152**, 774 (1966).

[13] W. Weibull, Ingenioersvetenskapsakad Handl. **151**, 45 (1939).

[14] P. M. Duxbury and P. L. Leath, J. Phys. A **20**, L411 (1987).